Supplementary Information

Equivalent circuit models for predicting electrical and gas output characteristics of CO_2 electrolysis cells

Yuki Kudo*, Akihiko Ono, Satoshi Mikoshiba and Ryota Kitagawa

Corporate Research & Development Center, Toshiba Corporation, Kawasaki, Kanagawa 212-8582, Japan

E-mail: yuki.kudo@toshiba.co.jp

Cell configuration

The cathode was prepared by spray coating Au/C catalyst powder onto carbon paper with a microporous layer (Avcarb, MB-30) [1]. Titanium non-woven fabric coated with an Ir-based catalyst (Becart) was used for the anode. The area of these electrodes was 16 cm^2 (cut to 4 × 4 cm). Here, electrode area, thickness, and CO_2 flow rate are discussed in detail as these are important parameters affecting cell performance. Increasing the electrode area and thickness has both positive and negative effects on cell performance, as described below. Due to the potential gradient between the anode and the cathode in the CO_2 reduction reaction, K^+ and solvating water (i.e., the electrolyte from the anode) can move to the cathode and reach the cathode flow channel. If the electrolyte is retained in the cathode flow channel, then flooding of the catalytic layer will likely occur, which may accelerate the hydrogen production reaction in the side reaction. This would reduce cell performance. For a given gas flow rate per unit area, the gas speed increases with an increasing electrode area and an increasing total gas flow rate (for the same groove depth of the cathode flow channel). The higher gas speed is advantageous for rapidly discharging the electrolyte reaching the channels, and the cell performance should improve as the electrode area is increased.

On the other hand, a large electrode area tends to cause in-plane non-uniformity in the clamping pressure of the components, which may result in a non-uniform current distribution and increase the cell voltage. A large power source and evaluation equipment are also required. We chose a medium-

sized electrode area of 16 cm^2 (= 4 × 4 cm) to allow for good cell performance and evaluation on a laboratory scale. A thicker electrode (i.e., a thicker gas diffusion layer [GDL]) would be advantageous for in-plane gas diffusion but disadvantageous for electrolyte evacuation in the thickness direction. Commercially available GDLs are around 200 to 400 μm thick, and we selected a GDL with a thickness of approximately 200 μm in the hope that it would favor electrolyte discharge. In this study, the gas flow rate was varied among four points for modeling purposes, as described below, but a higher CO_2 gas flow rate is advantageous for cell performance.

A commercially available anion exchange membrane (AEM; Versogen, PiperION HCO_3^- reinforced) separated the cathode and anode. The AEM was ion-exchanged twice with 500 mM KOH for 1 h. After washing the AEM with pure water, the membrane electrode assembly (cathode/membrane/anode) was stacked and clamped with flow channel plates (titanium), current collecting plates (SUS-coated gold), insulating plates (PTFE), cooling/heating plates (copper or aluminum), and clamping plates (SUS) as shown in Fig. 3. A gasket (PTFE), omitted from the figure, was placed around the electrode. Potential measurement is performed using a reference electrode in contact with the membrane. We measured the potential by touching a platinum foil (100 μm thick) as a Pt pseudo-reference electrode to the AEM on the cathode side, as shown in Fig. 3. Pt was used because it is chemically stable.

CO_2 electrolysis experiments

CO_2 (99.99 %) was supplied to the cathode channel using four different flow rate conditions, i.e., 40, 80, 120, 160 sccm (2.5, 5, 7.5, 10 sccm cm^{-2} per electrode area). The CO_2 was humidified with a bubbler to suppress salt precipitation in the cathode. The gas and electrolyte piping on the input side was heated to 50°C by a heater, which is not shown in Fig. 3. The gases output from the cathode and anode channels were diluted with Ar, and the flow rate was measured using a volumetric flow meter. Since the mixed gas is output from the cell, it is essential to measure the flow rate using a volumetric flow meter rather than a mass flow meter. The gas concentration output from the cell was analyzed using gas chromatography. The cell temperature was controlled by cooling or heating the cooling/heating plate, and the cell temperature was set to one condition of 50 °C. The anode flow channel was fed with 0.1 M $KHCO_3$ (99% Kanto Chemical) at a flow rate of 10 mL min^{-1}. A low anode electrolyte flow rate may lead to insufficient water supply to the anode catalyst due to the retention of generated O_2 bubbles, resulting in poor cell performance. The anode electrolyte flow rate was set to a value that did not affect cell performance.

A potentiostat (Bio-Logic Science Instruments, VMP-300 with 10A booster board) or DC power supply (KIKUSUI, PWR401L) was used to flow the current between the cathode and anode. The current-voltage characteristics were evaluated using the following measurement protocol.

(1) A constant current of 200 mA cm^{-2} is applied for 1 h as aging.

(2) The resistance is measured using the current interrupt method (from 200 mA cm^{-2} to 0 mA cm^{-2}). In our equivalent circuit model, the series resistance was approximated as a constant value, and the series resistance of the cathode $R_{s,cathode}$ (resistance between the cathode and the Pt) and the series resistance of the anode + the membrane resistance of the AEM $R_{s,anode} + R_{s,membrane}$ (resistance between the anode and the Pt) were applied as representative values.

(3) A staircase current (Table S1) is applied to measure the total current density dependence J_{total} of the cell voltage V_{cell}, the cathode potential V_c, the anode potential V_a, and the output gas concentration. Note that V_a includes the IR drop of the AEM. The duration of each step was 10 min. The range of J_{total} was varied with the CO_2 flow rate because CO_2 is consumed at low current density when the CO_2 flow rate is low (Table S2). Since CO concentrations were below the detection limit at 0.5 to 5 mA cm^{-2}, data above 10 mA cm^{-2} were used to calculate

the Tafel parameters.

Table S1 Staircase current (10 min per step)

Step	J_{total} (mA cm^{-2})	Step	J_{total} (mA cm^{-2})
1	0.5	13	250
2	1	14	300
3	2	15	350
4	5	16	400
5	10	17	450
6	20	18	500
7	40	19	550
8	60	20	600
9	80	21	650
10	100	22	700
11	150	23	750
12	200	24	800

Table S2 Range of the current density at each CO_2 flow rate

CO_2 flow rate (sccm cm^{-2})	Current density (mA cm^{-2})
2.5	0.5 – 400
5	0.5 – 600
7.5	0.5 – 700
10	0.5 – 800

The IR drop was removed, and the cathode and anode potentials for the reference hydrogen electrode (RHE), V_c (*vs.* RHE) and V_a (*vs.* RHE), were estimated using Eq. (S1).

$$V_{c\ or\ a}(vs.\,\mathrm{RHE}) = V_{c\ or\ a}(vs.\,\mathrm{Pt}) + V_{0,Pt} + \frac{RT}{F}ln(10)\mathrm{pH} \qquad \text{(S1)}$$

Here, $V_{0,\ Pt}$ is the potential versus the standard hydrogen electrode (SHE) of Pt pseudo-reference electrode, R is the gas constant, T is the temperature, and the subscripts c and a indicate the cathode and anode. Since the liquid permeated AEM, pH was assumed to be 7.8, equivalent to the electrolyte. The cell shown in Fig. S1 was used to compare the potential of the Pt pseudo-reference electrode and Ag/AgCl reference electrode (saturated KCl) by bringing two of them into contact with the AEM on the cathode side to investigate the electrode potential of the Pt pseudo-reference electrode. The average potential difference between the Pt pseudo-reference electrode and Ag/AgCl reference electrode in the low-current region used to estimate Tafel parameters in Fig. 5 had a small value of -7 mV. Therefore,

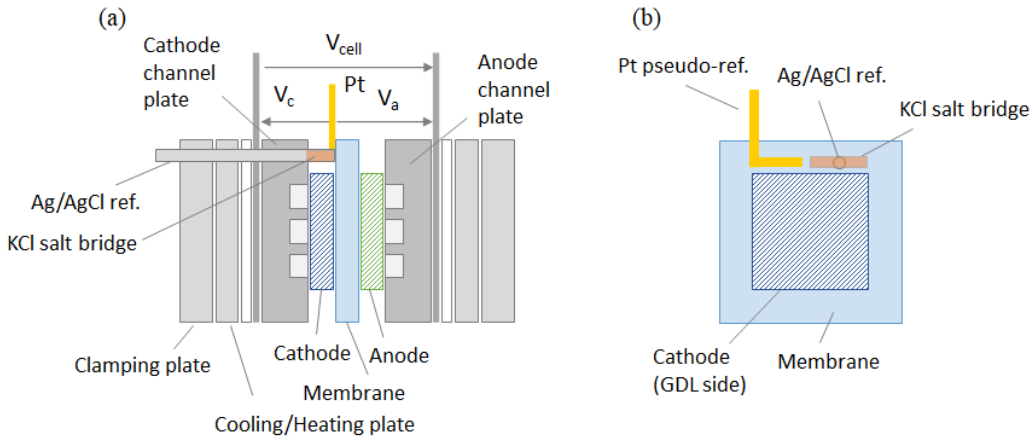

Fig. S1 Schematic drawing of CO_2 EC incorporating the Pt pseudo-reference electrode and the Ag/AgCl reference electrode (saturated KCl). (a) Cell configuration. (b) Location of the Pt pseudo-reference electrode and the Ag/AgCl reference electrode viewed from the back side of the cathode. The Pt pseudo-reference electrode was in contact with AEM. KCl salt bridges were placed between the Ag/AgCl reference electrode and AEM.

Table S3 Cathode potential

J_{total} (mA cm^{-2})	Cathode potential (V vs. Pt)	Cathode potential (V vs. Ag/AgCl)	Difference (V)
10.0	-1.046	-1.041	-0.005
20.0	-1.094	-1.088	-0.006
30.0	-1.127	-1.117	-0.010
40.0	-1.150	-1.141	-0.009

the potential of the Pt pseudo-reference electrode was estimated to be 167 mV versus SHE using the potential 174 mV versus SHE of the Ag/AgCl reference electrode. In the CO_2 flow rate dependence experiment, only Pt pseudo-reference electrode was used to measure the potential.

The overvoltages η_{CO}, η_{H_2}, and η_{O_2} of the CO evolution reaction, hydrogen evolution reaction, and O_2 evolution reaction were calculated from the standard electrode potential U, RHE reference cathode potential V_c, and anode potential V_a using the following equations.

$$\eta_{CO} = U_{CO} - V_c(vs.\,\mathrm{RHE}) \quad \text{(S2)}$$

$$\eta_{H_2} = U_{H_2} - V_c(vs.\,\mathrm{RHE}) \quad \text{(S3)}$$

$$\eta_{O_2} = V_a(vs.\,\mathrm{RHE}) - U_{O_2} \quad \text{(S4)}$$

The flow rate of each output gas ($M_{g,cathode\ or\ anode,out}$), the partial current density (J_g), and the Faradaic efficiency (FE_g) were calculated using the following equations.

$$M_{g,cathode\ or\ anode,out} = C_{g,cathode\ or\ anode}\frac{F_r}{V_{ntp}} \tag{S5}$$

$$J_g = M_{g,cathode,out} n_g F \tag{S6}$$

$$FE_g = \frac{J_g}{J_{total}} \tag{S7}$$

$$FE_{total} = FE_{CO} + FE_{H2} \tag{S8}$$

Here, C is the concentration, F_r is the volumetric flow rate, V_{npt} is the volume of ideal gas at NPT, the subscript g is the gas species (CO, H_2, O_2 in Eq. (S5); CO and H_2 in Eqs. (S6) and (S7)), n is the number of reaction electrons, and F is Faraday constant.

Effect of CO_2 flow rate for CO_2 EC performance

Figure S2 shows FE_{CO}, FE_{H_2}, and FE_{total} versus J_{total} for various CO_2 flow rates. When the CO_2 flow rate is low, FE_{CO} decreases, and FE_{H_2} increases because CO_2 is fully consumed at low current density. Conversely, when the CO_2 flow rate increases, the high FE_{CO} (> 90 %) region extends to the high current density side.

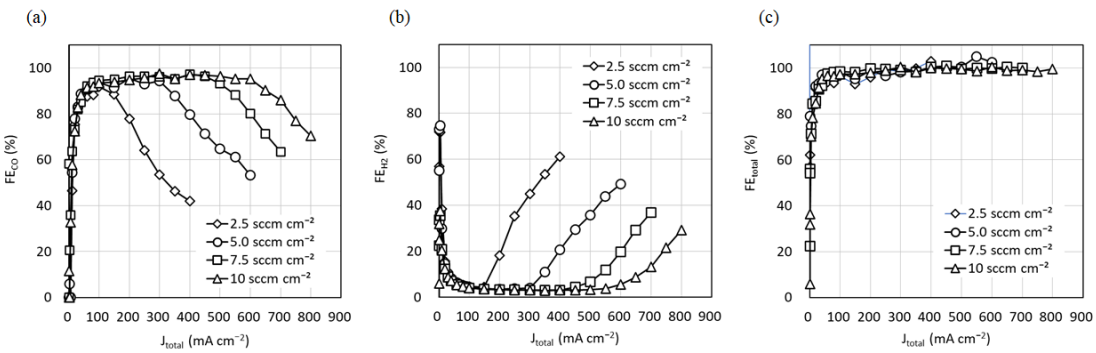

Fig. S2 FE_{CO}, FE_{H_2}, and FE_{total} versus J_{total} for various CO_2 flow rates

Figure S3 shows J_{CO} versus J_{total}. When the CO_2 flow rate is low, J_{CO} is limited to a low current density. We define limited J_{CO} at each CO_2 flow rate as $J_{CO,L}$, as shown in Fig. 4.

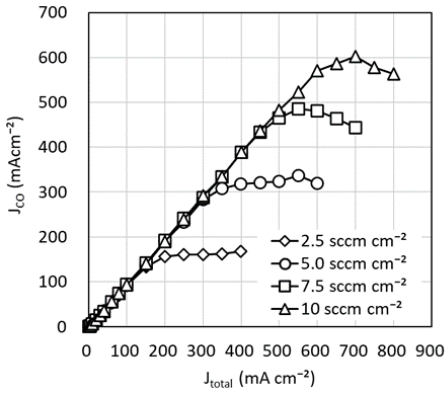

Fig. S3 J_{CO} versus J_{total} for various CO_2 flow rates.

Next, to verify the experimental results, we estimated the sum of CO_2 flow rate output from the cathode and anode with the CO_2 consumption flow rate for the CO_2 reduction reaction.

$$F_{r,CO_2,output\ and\ consumption} = \left(M_{CO_2,cathode,out} + M_{CO_2,anode,out} + M_{CO_2,cathode,consumption}\right)V_{ntp} \quad \text{(S9)}$$

As shown in Fig. S4, for a wide range of current densities, the sum of the CO_2 output from the cathode and anode with the CO_2 consumption flow rates was close to the input CO_2, with a small difference of less than 5%.

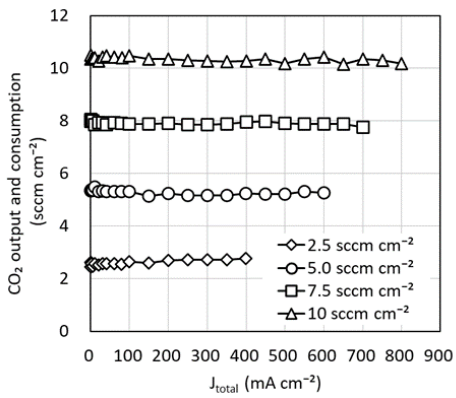

Fig. S4 Sum of CO_2 output from the cathode and anode flow rates with CO_2 consumption versus J_{total}.

Simulation of faradaic efficiency and cell voltage of CO_2 EC

Figure S5 compares simulated and measured data for faradaic efficiency and cell voltage for the CO_2 flow rates of 2.5, 7.5, and 10 sccm cm^{-2} using the parameters determined at the CO_2 flow rate of 5

sccm cm^{-2}. The simulation reproduces the experimental behavior well, which means that our equivalent circuit model can be used to predict the output characteristics of the CO_2 EC.

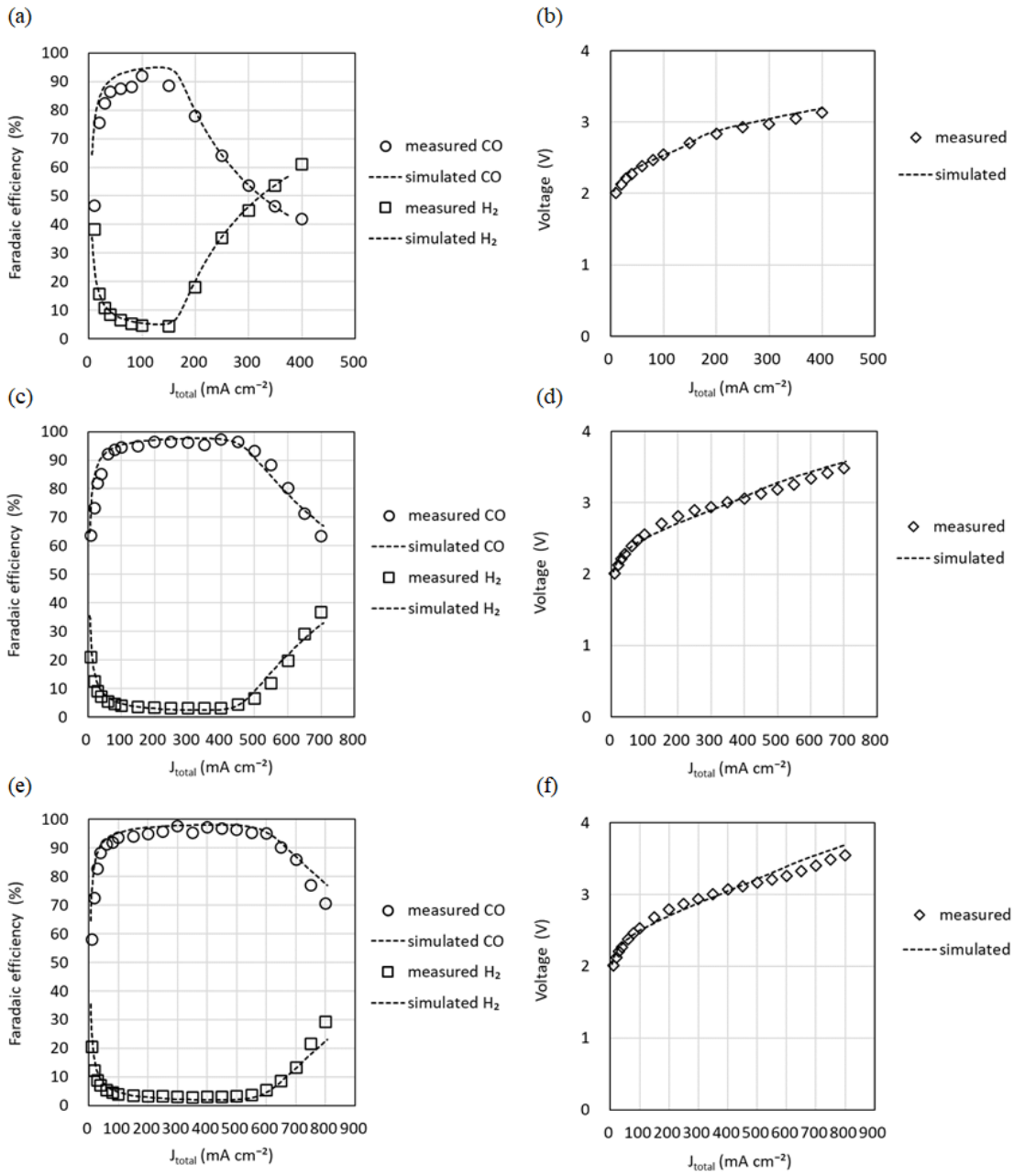

Fig. S5 Faradaic efficiency and cell voltage versus total current density (J_{total}) for four CO_2 input flow conditions. (a), (b) CO_2 input: 2.5 sccm cm^{-2}. (c), (d) CO_2 input: 7.5 sccm cm^{-2}. (e), (f) CO_2 input: 10 sccm cm^{-2}.

Mass balance of $C_xH_yO_z$ evolution reaction

In the main text, we discussed mass balance when the CO is generated from CO_2. Here, we further generalize and supplement the case where $C_xH_yO_z$ is produced from CO_2.

The reaction equation for the evolution of $C_xH_yO_z$ by CO_2 reduction reaction is expressed as follows.

$$x\mathrm{CO_2} + a\mathrm{H_2O} + n_{C_xH_yO_z}\mathrm{e^-} \rightarrow \mathrm{C}_x\mathrm{H}_y\mathrm{O}_z + n_{C_xH_yO_z}\mathrm{OH^-} \quad \text{(S10)}$$

$$a = 2x + y - z \quad \text{(S11)}$$

$$n_{C_xH_yO_z} = 4x + y - 2z \quad \text{(S12)}$$

The $C_xH_yO_z$ output from the cathode is expressed using the partial current density used for the $C_xH_yO_z$ evolution reaction ($C_xH_yO_z$ ER),

$$M_{C_xH_yO_z,cathode,out} = \frac{J_{C_xH_yO_z}}{n_{C_xH_yO_z}F} \quad \text{(S13)}$$

where M is the molar flow rate mol s^{-1} cm^{-2}, J is the current density A cm^{-2}, n is the number of reactive electrons, and F is Faraday's constant C mol^{-1}. In an anion-transfer type cell, some of the CO_2 input to the cathode becomes CO_3^{2-} or HCO_3^-, which moves to the anode by drift or diffusion and is converted again to CO_2. Therefore, the unreacted CO_2 output from the cathode is the CO_2 input to the cathode minus the CO_2 used for $C_xH_yO_z$ ER and the CO_2 output from the anode, which can be expressed as follows.

$$M_{CO_2,cathode,out} = M_{CO_2,cathode,in} - xM_{C_xH_yO_z,cathode,out} - M_{CO_2,anode,out} \quad \text{(S14)}$$

The CO_2 used for $C_xH_yO_z$ ER can be expressed in terms of $C_xH_yO_z$ flow rate using the molar ratio x between the CO_2 and $C_xH_yO_z$, as shown in Eq. (S10).

Since the charges of CO_3^{2-} and HCO_3^- are differ by a factor of two, as shown in Eqs. (5) and (6), the CO_2 (per reaction electron number) output from the anode depends on the ion species. This paper proposes a model that accounts for CO_3^{2-} and HCO_3^- migration by expressing the fraction of CO_3^{2-} that moves from the cathode to the anode as G (fraction of $HCO_3^- = 1 - G$). Using G, the CO_2 output from the anode can be expressed as follows.

$$M_{CO_2,anode,out} = \frac{J_{C_xH_yO_z}}{2F}(2 - G) \quad \text{(S15)}$$

If the CO_2 output from the cathode is zero, the CO_2 flow rate used to generate $C_xH_yO_z$ and the CO_2 flow rate output from the anode can be expressed as follows.

$$\frac{M_{CO_2\ to\ C_xH_yO_z,cathode,out}}{M_{CO_2,cathode,in}} = \frac{x\left[\frac{n_{C_xH_yO_z}}{2}(1+G)+x\right]}{\left(x+\frac{n_{C_xH_yO_z}}{2}\right)\left(x+n_{C_xH_yO_z}\right)} \tag{S16}$$

$$\frac{M_{CO_2,anode,out}}{M_{CO_2,cathode,in}} = \frac{\frac{n}{2}\left[x(2-G)+n_{C_xH_yO_z}\right]}{\left(x+\frac{n_{C_xH_yO_z}}{2}\right)\left(x+n_{C_xH_yO_z}\right)} \tag{S17}$$

The results of the calculations according to Eqs. (S16) and (S17) for various $C_xH_yO_z$ evolution reactions are shown in Table S4.

Table S4 Ratio of the CO_2 flow rate used for $C_xH_yO_z$ evolution and the CO_2 flow rate output from the anode (when CO_2 output from the cathode is zero)

							G = 1 (CO_3^{2-} transport)		G = 0 (HCO_3^- transport)	
$C_xH_yO_z$		x	y	z	a	n	$\frac{M_{CO_2\ to\ C_xH_yO_z,cathode,out}}{M_{CO_2,cathode,in}}$	$\frac{M_{CO_2,anode,out}}{M_{CO_2,cathode,in}}$	$\frac{M_{CO_2\ to\ C_xH_yO_z,cathode,out}}{M_{CO_2,cathode,in}}$	$\frac{M_{CO_2,anode,out}}{M_{CO_2,cathode,in}}$
Carbon monoxide	CO	1	0	1	1	2	0.500	0.500	0.333	0.667
Formic acid	HCOOH	1	2	2	2	2	0.500	0.500	0.333	0.667
Methanol	CH_3OH	1	4	1	5	6	0.250	0.750	0.143	0.857
Methane	CH_4	1	4	0	6	8	0.200	0.800	0.111	0.889
Ethylene	C_2H_4	2	4	0	8	12	0.250	0.750	0.143	0.857
Ethanol	C_2H_5OH	2	6	1	9	12	0.250	0.750	0.143	0.857
Ethane	C_2H_6	2	6	0	10	14	0.222	0.778	0.125	0.875
Propanol	C_3H_7OH	3	8	1	13	18	0.250	0.750	0.143	0.857
Ethylene glycol	$C_2H_6O_2$	2	6	2	8	10	0.286	0.714	0.167	0.833

$C_xH_yO_z$ limiting current density ($J_{CxHyOz,L}$)

The maximum amount of CO_2 available for $C_xH_yO_z$ ER is the amount of CO_2 input from the cathode minus the amount of CO_2 transferred to the anode. In other words, $J_{CxHyOz,L}$ is limited by the maximum amount of CO_2 available for $C_xH_yO_z$ ER. The relationship between $J_{CxHyOz,L}$, and the CO_2 flow rate input to the cathode can be expressed as follows.

$$J_{C_xH_yO_z,L} = \frac{x\left[\frac{n_{C_xH_yO_z}}{2}(1+G)+x\right]}{\left(x+\frac{n_{C_xH_yO_z}}{2}\right)\left(x+n_{C_xH_yO_z}\right)} n_{C_xH_yO_z} F M_{CO_2,cathode,in} \tag{S18}$$

Using this mass balance and the limiting current density equations of the $C_xH_yO_z$ ER, our equivalent circuit model can be applied to CO_2 ECs that produce various gases and liquids from CO_2.

Reference

[1] Kofuji, Y. et al. "Efficient Electrochemical Conversion of CO_2 to CO Using a Cathode with Porous Catalyst Layer under Mild pH Conditions" *Chem. Lett*., 2021, **50**, 482-484